

Technical Paper by B. Chareyre, L. Briançon, and P. Villard
THEORETICAL VERSUS EXPERIMENTAL MODELING
OF THE ANCHORAGE CAPACITY OF GEOTEXTILES IN
TRENCHES

ABSTRACT: The behavior of the anchorage of geotextile sheets at the top of a slope is a decisive factor when determining the dimensions of geosynthetic lining systems on slopes. In order to optimize the geometry of the structures in question (to reduce the area taken up by the anchorage at the top of the slope), anchorage solutions using trenches of varying forms are sometimes used. Calculating the required dimensions of this anchorage remains problematic. To improve knowledge of the behavior of anchor trenches, experimental studies and numerical studies were developed. Full-scale pull-out tests were carried out on anchored geotextile sheets (run-out anchorage and anchor trenches). Two types of soil were studied: sand and sandy silt. The numerical modeling proposed was based on the Discrete Element Method (DEM). This method is particularly well suited to the problem being addressed, for it enables consideration of major movements and large-scale deformation of the soil (rotation, compression, and lifting) as well as large displacements between the geotextile and the soil. Comparisons between the experimental and numerical results provide practical conclusions concerning anchorage mechanisms.

KEYWORDS: Anchorage, Trench, Geotextile, Experimentation, Discrete element modeling, Granular material.

AUTHORS: B. Chareyre, Ph.D. Student, Lirigm, Université Joseph Fourier, 38041 Grenoble, Cedex 9, France, Telephone: 33/0476828080, Telefax: 33/0476828072, E-mail: Bruno.chareyre@ujf-grenoble.fr; L. Briançon, Ph.D. Student, Cemagref, Groupement de Bordeaux, 50-avenue de Verdun, 33612-Cestas Cedex, France, Telephone: 33/0557890800, Telefax: 33/0557900801, E-mail: laurent.briancon@bordeaux.cemagref.fr; and P. Villard, Assistant Professor, Lirigm, Université Joseph Fourier, 38041 Grenoble, Cedex 9, France, Telephone: 33/0476828052, Telefax: 33/0476828070, E-mail: Pascal.villard@ujf-grenoble.fr.

PUBLICATION: *Geosynthetics International* is published by the Industrial Fabrics Association International, 1801 County Road B West, Roseville, Minnesota 55113-4061, USA, Telephone: 1/612-222-2508, Telefax: 1/612-631-9334. *Geosynthetics International* is registered under ISSN 1072-6349.

DATE: Original manuscript submitted 19 December 2001, revised version received 28 January 2002, and accepted 1 February 2002. Discussion open until 1 February 2003.

REFERENCE: Chareyre, B., Briançon, L., and Villard, P., 2002, "Theoretical Versus Experimental Modeling of the Anchorage Capacity of Geotextiles in Trenches", *Geosynthetics International*, Vol. 9, No. 2, pp. 97-123.

1 INTRODUCTION

There are currently a large number of applications implementing geosynthetic liner systems on slopes (e.g., canal banks, reservoirs, and landfills) comprising geomembranes, geotextiles, geogrids, and geonets. In some cases, geotextiles are used as reinforcement to reduce tensile forces in geomembranes. The long-term stability of these structures may depend on the efficiency of the anchorage of geotextile sheets. Depending on the space available at the top of the slope and on the loads applied, the anchorage systems may take on different shapes (Figure 1): run-out anchorage or digging trenches of varying geometry (vertical embedding and L-shaped anchorage geometries research are presented in this paper).

Calculating anchorage capacities (i.e., the force T_{max} required to pull the sheet out) using the geometric characteristics of the anchorage and the friction characteristics of the materials used remains a difficult task because the forces and stresses that develop at each curved portion of the anchorage are complex.

Few experiments have been carried out on anchor trenches at the top of slopes. The existing reported studies were carried out on geomembranes in situ (Imaizumi et al. 1997) or by adapting an existing laboratory apparatus (Koerner and Wayne 1991).

The first analytical formulae put forward to calculate the dimensions of anchorage (Hulling and Sansone 1997) assumed that the loads on the anchorage were taken up only by friction on the linear parts of the geosynthetic without the existence of angle effects. The friction loads were governed by a Coulomb-type law: $\tau = a + \sigma_n \tan \delta$ where a and δ are the strength and the friction angle of the interface in question, respectively. The parameter σ_n is the normal stress acting on the interface, equal to σ_v (vertical stress) on the horizontal portions of the sheet, and equal to σ_h (horizontal stress) for the vertical portions of the sheet. The parameter σ_h is taken to equal $K_0 \sigma_v$, and K_0 is the coefficient of earth pressure at rest.

These methods were then adapted to the cases of run-out anchorage and vertical embedding (Koerner 1998, pp. 487-494) by taking into consideration the angle of incline of the tensile force along the slope. In this case, Koerner (1998), assumed that the traction of the geosynthetic along the slope induced, on the horizontal section of the sheet, additional normal stresses at the soil-geosynthetic interface (equivalent to the vertical component of the tensile force), hence, an increase in the interface friction forces.

Analytical formulae, taking into account the influence of the change of angle, have been proposed by different authors (Guide technique 2000). In these formulae, at each

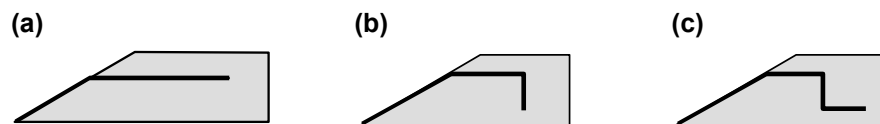


Figure 1. Types of anchors studied: (a) run-out anchorage; (b) vertical embedding; (c) L-shaped anchor.

change of direction of the geosynthetic sheet, the anchorage capacity is multiplied by a factor equal to $e^{\lambda \tan \delta}$; λ being the angle of the change in direction expressed in radians and δ the interface friction coefficient. The value of the factor is based on the limit equilibrium of a geosynthetic resting on a circular arc; one demonstration of this may be found in the paper by Hryciw (1990).

Experimental pull-out tests were carried out on geosynthetic sheets at the Cemagref (research institute for agricultural and environmental engineering) in Bordeaux, France, with the aim of validating the proposed formulae. The first comparisons made (Briançon et al. 2000) showed that no single formula was capable of describing the behavior of all types of anchorage, even though some were close to the experimental results in certain cases.

This being the case, it seemed necessary to consider a more complex form of modeling that could explain the failure of the analytical formulae in question. A discrete element calculation method was chosen because discrete elements can provide good discretization of granular media and can accommodate large-scale modifications in the soil.

2 EXPERIMENTATION

2.1 General

The experimental tests were carried out at Cemagref on a large anchorage bench offering the possibility of performing full-scale, pull-out tests. Preliminary tests carried out using sand (Briançon et al. 2000, Briançon 2001) showed the repeatability of the tests, the influence of the slope angle, and the influence of the trench dimensions. Complementary tests with specific instrumentation were carried out on sandy silt and on sand, in order to provide a better understanding of the phenomena involved and for comparison purposes, i.e., comparisons with modelling results

2.2 Experimental Apparatus

The anchorage bench (Figure 2) comprised an anchor block of a width of one meter and a traction system. The dimensions of the anchorage zone allowed for an anchor trench with a total depth ($D + H$) equal to 1 m and a length ($L + B$) of up to 1.2 m. The traction system consisted of a winch, with a maximum capacity of 50 kN, and a pulley that enabled tensile forces to be applied on the geotextile at incline angles, β , between 0° and 35° . This traction system was fixed onto the geotextile using a metal clamp. The slope incline was made slightly higher than β (approximately 2° higher) to create a space between the soil and the clamp. The geotextile remained in contact with the slope at the top, due to a small deformation of the soil in the early stages of the test.

To limit edge effects, the side walls of the anchorage bench were covered with a smooth, polypropylene geomembrane. The sand-geomembrane friction angle was approximately 20° . The soil was installed in successive layers and then compacted. In the upper section of the anchor block (top layer of soil with a thickness H) a space of approximately 10 mm was left between the soil and the side walls of the anchorage

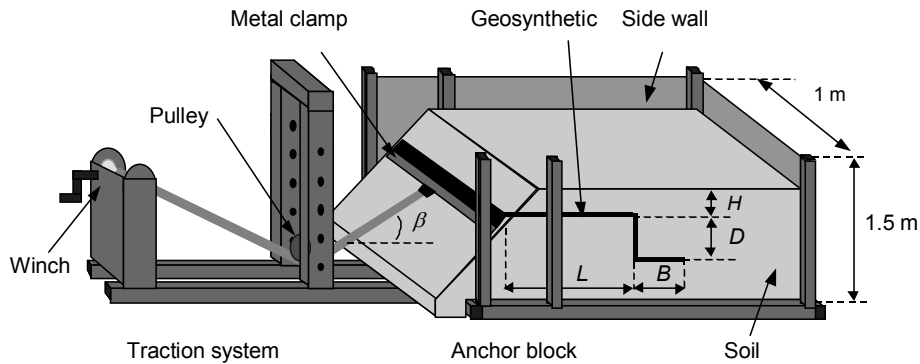


Figure 2. Experimental apparatus.

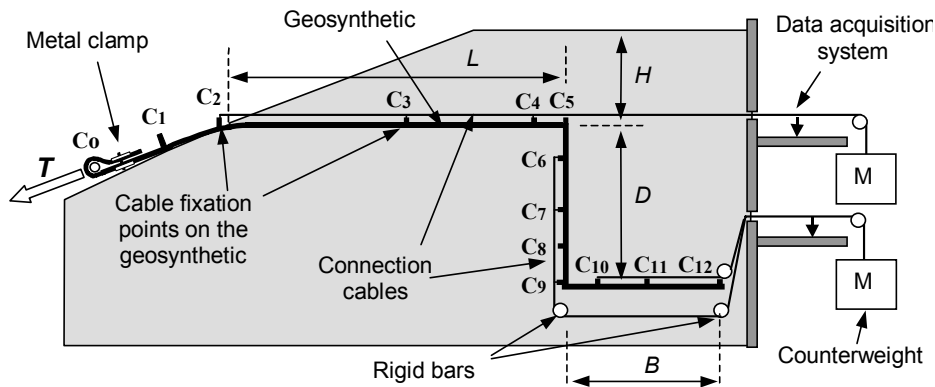


Figure 3. System for measuring displacements of the geosynthetic with an L-shaped anchor.

bench to avoid any contact and any friction that might have resulted from the large displacements of the top layer of soil during the test.

2.3 Instrumentation

The tensile force T and the displacement U_0 of the traction cable were measured during pull-out via sensors fixed onto the traction system at point C_0 . In the anchorage zone (Figure 3), a cable measuring system was used to monitor displacements of the geotextile at different points (C_1 to C_{12}). The cables could slide through the flexible sleeves isolating them from the soil, were fixed to the geotextile sheet, and were tensioned using counterweights (5 N each). For points C_6 to C_{12} , the sleeves were brought and held in position using rigid bars fixed to side walls (Figure 3). The overall resisting force due to cables/sleeves friction and counterweights was estimated to be less than

90 N, which is negligible when compared to the pull-out force.

A graphic acquisition system positioned at the rear of the test bench was used to measure displacements during pull-out. In certain cases, the movement of the soil could be observed due to columns of colored sand positioned in the anchorage zone before starting the test. After the geotextile sheet had been pulled out, the area of the soil directly above the sand columns was meticulously cut into sections to analyze the failure mechanisms and the displacements of the soil.

2.4 Characteristics of the Materials Used

2.4.1 Geotextiles

The following two different types of geotextiles of varying tensile stiffness, all 1 m wide, were used for the pull-out tests:

- A nonwoven, needle-punched geotextile (GTX₁) (Bidim P50) with tensile stiffness $J = 80$ kN/m (at 5% strain) and tension failure $T_r = 30$ kN/m (at 85% strain).
- A nonwoven, needle-punched geotextile (GTX₂), reinforced in one direction (Bidim Rock 75) with tensile stiffness J in the direction of the reinforcement of 624 kN/m (at 12% strain) and tension failure $T_r = 95$ kN/m (at 12% strain).

2.4.2 Soils

The following two soils, a sand and a sandy silt, were used for comparison purposes:

- The sand was fine-rolled with particles size ranging from 0.08 to 2.5 mm. Its unit weight once installed, γ_d , was 16.2 ± 0.2 kN/m³. Its water content, w , varied from 2 to 4%. Using triaxial tests, an internal friction angle $\phi = 41^\circ$ (residual value) and cohesion $c = 0$ were measured. The residual friction angle was considered relevant since anchorages exhibit a progressive failure.
- The sandy silt was a fine soil (70% of the particles smaller than 80 μm) with a liquid limit $W_L = 30$, a plastic limit $W_P = 22$, and a plasticity index $I_P = 7.6$. Its unit weight once installed, γ , was 18.5 kN/m³ for a water content $w = 23\%$. Its mechanical characteristics, measured in undrained consolidated triaxial tests, resulted in a residual friction angle $\phi' = 35^\circ$ (no peak) and cohesion $c' = 5$ kPa.

2.4.3 Interfaces

The characteristics of the soil-geotextile interface (friction angle, δ , and adhesion, a) were determined using an inclined plane and a shear box in accordance with the French Standard (NF P 84-522) and the draft European standard (prEN ISO 12957-1 and prEN ISO 12957-2) for determining geotextile interface friction characteristics on an inclined plane with a shear box. The results were identical for the two geotextiles tested (similar texture, except for the reinforcements). Since no peak was found, the following residual values were given:

- Sand-GTX interface: $\delta = 37^\circ$ and $a = 0$ kPa.

- Sandy silt-GTX interface: $\delta = 30^\circ$ and $a = 0$ kPa.

2.5 Types of Tests Performed

The following two series of tests were compared with the model:

- The first series of tests (sand and GTX₁) focused on determining the influence of the slope angle, β , on the geotextile pull-out force and was performed on run-out anchorage for $\beta = 0^\circ, 7^\circ, 15^\circ, 20^\circ, 27^\circ,$ and 30° , for a height of soil $H = 0.25$ m, and for a sheet length $L = 1.5$ m.
- The second series of tests (sand, sandy silt, and GTX₂) targeted the understanding of anchorage mechanisms and comprised run-out anchorage tests (S₁, S₁' , T₁ and T₁'), vertical embedding tests (S₂ and T₂), and L-shaped anchorage tests (S₃ and T₃). The main parameters of the tests performed are all presented in Table 1.

2.6 Experimental Results

2.6.1 The Influence of β on Resistance of Run-Out Anchorage (First Test Series)

In the tests on run-out anchorage (Briançon 2001), the geotextile pull-out force, T , reached a maximum, T_{max} , corresponding to the anchorage capacity of the set-up being studied. The comparison between the different tests (sand and GTX₁) was made at this maximum force (Table 2 and Figure 4). According to the results, it appears that the maximum force applied to the geotextile increases markedly as the slope angle increases and that this increase in relation to a horizontal traction test reaches 22% for $\beta = 30^\circ$. Note that T_h , the horizontal component of the pull-out force (Table 2), is approximately constant for any β value.

Table 1. Values of the test parameters.

Test	Type of soil	β (°)	H (m)	L (m)	D (m)	B (m)
T1	Sandy silt	0	0.3	1.1	0	0
T1'		20	0.3	1.1	0	0
T2		20	0.3	1.1	0.5	0
T3		20	0.3	1.1	0.5	0.5
S1	Sand	0	0.3	1.1	0	0
S1'		20	0.3	1.1	0	0
S2		20	0.3	1.1	0.5	0
S3		20	0.3	1.1	0.5	0.5

Table 2. Experimental results of the run-out tests.

β (°)	0	7	15	20	23	27	30
T_{max} (kN)	3.57	4.02	3.92	4.13	4.23	4.28	4.37
T_h (kN)	3.57	3.99	3.78	3.88	3.89	3.81	3.78

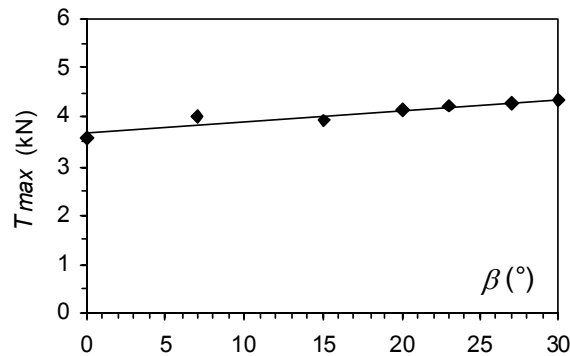


Figure 4. Influence of angle β on anchorage capacity.

2.6.2 Trench Anchorage Studies (Second Test Series)

The results of the anchor trench tests carried out with the sand, sandy silt, and Geotextile GTX₂ (second test series) are presented in Table 3. The results obtained show that the anchorage capacities are much greater with the sandy silt, despite the weaker interface characteristics ($\delta = 30^\circ$ for the sandy silt-GTX₂ interface, compared with $\delta = 37^\circ$ for the sand-GTX₂ interface). These results show that the soil plays a major role in anchorage mechanisms and that it is not enough to take into consideration only the interface friction characteristics when determining anchorage capacities.

The measurements made during the tests were used to obtain measurements of the forces, T , at the top of the slope and the displacements of the geotextile in relation to the displacement U_θ of the traction cable (sensor C₀). As a comparison, the results obtained for L-shaped anchors with sand (S₃) and sandy silt (T₃) are presented in Figures 5 and 6.

In Figure 5 (sand and GTX₂), note that the curve representing the displacement of sensor C₄ in relation to the displacement of sensor C₀ is composed of four segments with differing angles, highlighting the following different stages in the mobilization of friction along the geotextile in the trench:

- $0 \text{ m} < U_\theta < 0.03 \text{ m}$: no displacement of sensor C₄. This stage corresponds to the gradual tensioning of the geotextile on the horizontal section of the anchorage.
- $0.03 \text{ m} < U_\theta < 0.12 \text{ m}$: sensor C₄ begins to move and the slope of this segment is

Table 3. Results of the anchorage tests.

Tests with sand		Tests with sandy silt	
Type of test	T_{max} (kN)	Type of test	T_{max} (kN)
S1	2.67	T1	5.05
S1'	3.33	T1'	6.66
S2	8.29	T2	12.63
S3	14.00	T3	27.85

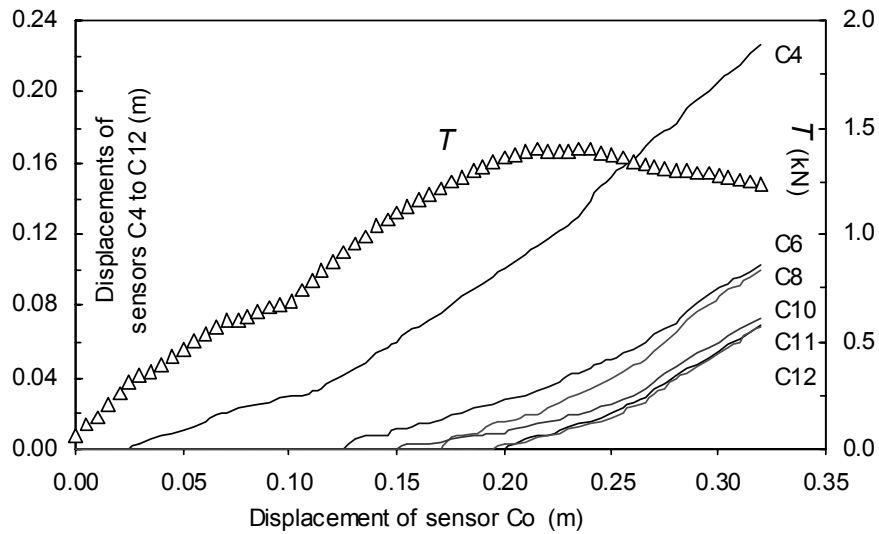


Figure 5. Results of anchorage test S3 (sand + GTX2).

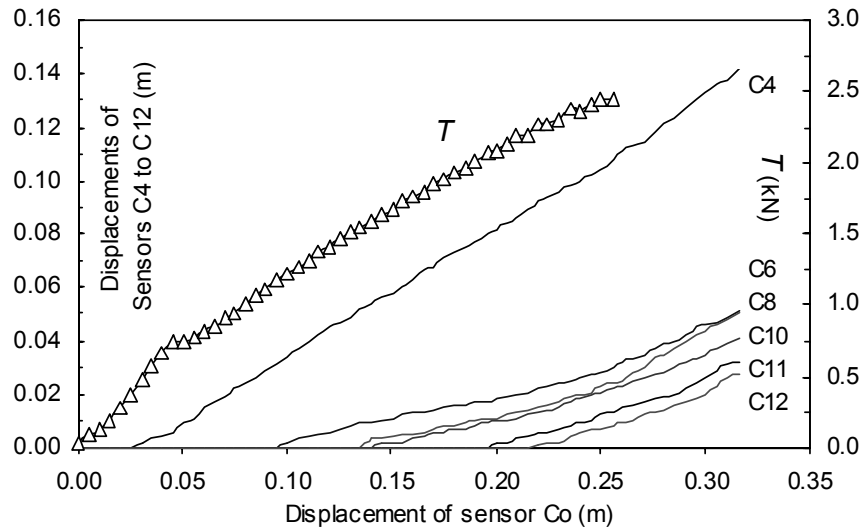


Figure 6. Results of anchorage test T3 (sandy silt + GTX2).

slight. This stage corresponds to the rounding out of the upper corner of the trench and ends when sensor C_6 begins to move.

- $0.12 \text{ m} < U_0 < 0.235 \text{ m}$: the slope of this segment is steeper than that of the previous one. This stage corresponds to the gradual tensioning of the geotextile in the trench (segments of lengths D and B) and to the lifting of the soil in the bottom cor-

ner of the trench. At the end of this stage, the tensile force applied to the geotextile reaches its maximum. Simultaneously, the end of the geotextile sheet (sensor C_{12}) begins to move. It should be noted that this occurs simultaneously in all the tests carried out on sand.

- $U_0 > 0.235$ m: this stage corresponds to the sliding of the geotextile out of the trench, and the increases in the displacements of all the sensors are identical.

Figure 6 (sandy silt and GTX₂) shows a somewhat similar anchorage behavior. It should be noted, however, that in this test, the end of the sheet moved (sensor C_{12}) before the force applied to the geotextile had reached its maximum. This behavior is typical of sandy silt and was observed in all the tests carried out on this material.

The photos in Figure 7 highlight the differences in behavior that could be observed at the top corners of the anchor trenches. These photos were taken at the end of the tests when the pull-out force applied to the geotextile had reached its maximum. It can be observed in Figure 7a that the sand at the top corner has been greatly smoothed down (large deformation of the columns of colored sand that were initially vertical) and that there is a very localized sliding plane in the sand under the geotextile. This failure mechanism does not appear in Figure 7b for the sandy silt, which is deformed by mass movement.

3 NUMERICAL MODELING BY THE DISCRETE ELEMENT METHOD

3.1 Presentation of the Modeling Method

3.1.1 Choice of the Discrete Element Method

It was decided to simulate the anchorage tests using the Discrete Element Method (DEM). This method, developed by Cundall and Strack (1979), models granular media

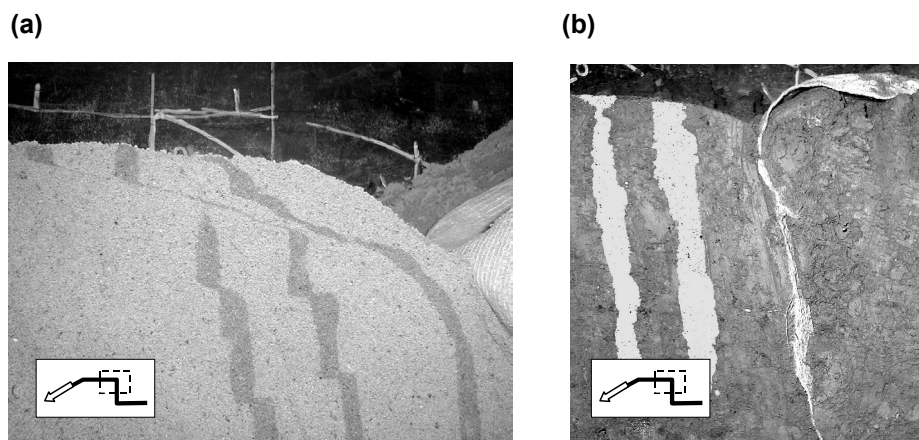


Figure 7. Soil deformation at the upper corner of the anchor: (a) sand; (b) silt.

using a set of independent elements of varying sizes interacting at contacts. The principle of discrete simulation allows for unlimited deformation and displacements, as well as for macroscopic discontinuities within the model. The final state may therefore be radically different from the initial state. For these reasons, DEM was considered well suited to the task of simulating anchorage tests involving major geometrical changes during the course of calculations, notably at the soil-geotextile interface. On the other hand, modeling on the scale of individual particles is controlled by local laws of behavior at particle contacts. This prevented direct introduction of laws of behavior such as those defined by the mechanics of continuous media. A change of scale is required in order to get from the measurable geotechnical parameters (friction, cohesion) to the parameters of the numerical model.

3.1.2 The Model and Numerical Resolution

Anchorage was considered to be a two-dimensional problem. The model used (calculations performed with the PFC^{2D} software program developed by Itasca) was a particular application of DEM involving cylindrical particles (of variable sizes), thus making it analogous to the physical model of Schneebeli (1956). The contacts between particles behave perfectly elastic plastic. The elastic behavior of the contact was defined by two parameters: normal stiffness k_n and shear stiffness k_s (Figure 8). Two contact failure criteria were defined: one under tension, characterized by a tensile strength limit, a_n , the other in relation to shear forces and characterized by shear strength, a_s (independent of normal force), or by a friction angle, μ . For cylindrical particles, the normal and shear stiffness and strength were given by unit length. The force and displacement boundary conditions were imposed using rigid walls. The element-wall contacts were defined in a similar way to that used for contacts between particles. Numerical resolution was based on the discretization of time into intervals Δt . Since all of the forces applied to each particle were known, the displacements and rotations could be integrated on Δt following an explicit, finite difference formulation of the laws of dynamics. The contact forces were then re-calculated for the succeeding time step.

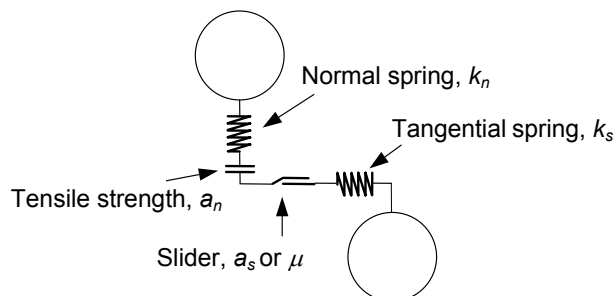


Figure 8. Contact model.

3.2 Determining the Parameters for Modeling a Soil

3.2.1 General

Not enough is known of the way in which the micro-mechanical parameters of a set of particles correspond to its global behavior. For this reason, determining the adequate parameters remains the main difficulty in terms of discrete element modeling, especially when the experimental data (friction and cohesion) is only macroscopic. Faced with the lack of theoretical solutions, it was decided to establish the match between the micro and macro characteristics of the soil by simulating biaxial compression tests. An extensive parametric study of these compression tests, carried out with different particle sizes, enabled the equivalence between the micro-mechanical parameters (porosity and contact parameters) and the parameters of the equivalent continuous medium (friction angle, cohesion, and global elastic behavior) to be established. The calculations performed showed that the friction angles obtained with the circular elements of DEM gave soil internal friction angles, ϕ , that were low compared with those obtained with sand in the experiment (41°). Higher ϕ values were obtained by making assemblies of two particles bonded together by rigid contact conditions. The assemblies used to model anchorage and biaxial compression tests were formed by two cylindrical particles of diameters d and d' , respectively, assembled in pairs, where $p = d'/d$ with $d' < d$ and $l = d' + d$. Two assembly sizes were used to generate the samples: small assemblies with length l_1 and large assemblies with length l_2 equal to $2 \times l_1$.

3.2.2 Simulation of a Biaxial Compression Test

Several important stages are required to simulate a biaxial compression test: generating the sample, achieving the desired porosity, and then the compression itself.

Generation of the Sample. The positions of the particles were chosen randomly within the field bounded by four rigid walls defining the contours of the test sample.

Achieving the Desired Porosity. After the particle positioning phase, the density of the sample is generally low (no inter-granular contact). There are then two stages in order to achieve a precise porosity: gradually increasing the size of the particles and then increasing the density of the sample by reducing inter-granular friction until the desired porosity is reached (during this phase, a constant isotropic stress was maintained by slightly adjusting the size of the particles). Once the assembly was stable and had the desired porosity n , the definitive values of the friction and strength parameters were entered.

Biaxial Compression. Biaxial compression was simulated by imposing a translation speed V on the upper wall while the interlocked side walls maintained a constant lateral stress σ_0 (Figure 9). The four walls were non-frictional. A compression speed that was sufficiently slow to eliminate dynamic phenomena interference with the results was chosen. The strains and stresses were deduced directly from the displacements and the forces exerted on the walls. It should be noted that, due to the random character of

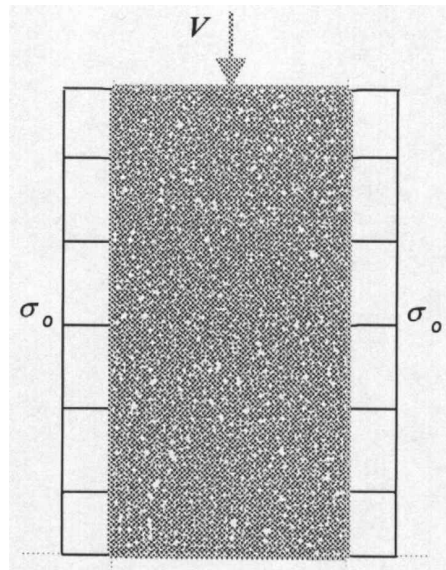


Figure 9. Geometry of the sample.

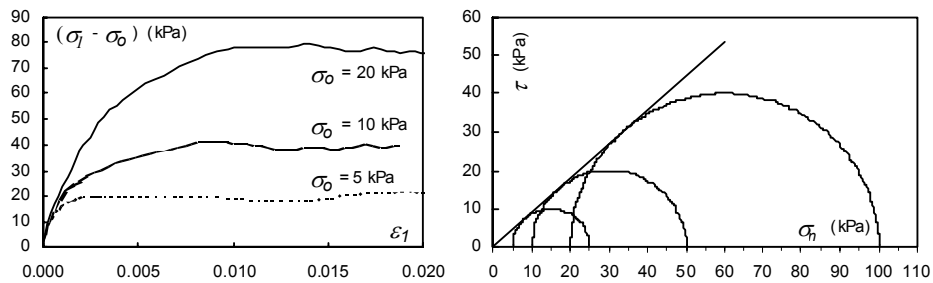


Figure 10. Results of a biaxial compression test with parameters selected to model the soil.

the arrangements, two successive simulations of the same problem never give exactly the same result, if the particle generation phases are distinct. Each model proposed was therefore simulated several times, to assess how representative the results were and to obtain average curves and values.

Results of a biaxial compression test simulation are presented in Figure 10. The parameters selected to model the soil are those of Table 4, which reproduce the behavior of a noncohesive material with friction $\phi = 41^\circ$.

Table 4. Parameters selected to model the soil.

Soil modeling parameters	Value
Particle size (two sizes of particle assembly)	
Length l_1 of the small assemblies (m)	l
Length l_2 of the large assemblies (m)	$2 \times l$
Proportion of the small assemblies (mass)	50%
Proportion of the large assemblies (mass)	50%
Ratio p of the assemblies	0.9
Micro-mechanical parameters	
Tensile stiffness, k_n^{ss} (kN/m ²)	1×10^5
Shear stiffness, k_s^{ss} (kN/m ²)	0.5×10^5
Inter-particle friction angle, μ^{ss} (°)	40.4
Shear strength, a_s^{ss} (N/m)	0
Tensile strength, a_n^{ss} (N/m)	0
Porosity, n	0.2

3.3 Determining the Parameters for Modeling the Geotextile

Geotextiles are thin elements characterized by a tensile stiffness J and a tension at failure T_r . The absence of bending strength means that, when a force is applied in a direction perpendicular to the geotextile plane, the geotextile deforms like a membrane. In this case, it was decided to model the geotextile by successively assembling particles of the same diameter d^g , bonded to each other by contact conditions (contacts have no bending strength). In this precise case, one can obtain an analytical relation between the physical parameters and the modeling parameters by considering the action of direct tension on this assembly. The result is that the tension at failure, T_r , of the geotextile corresponds to the tensile strength, a_n^{gg} , of the bonds between the particles ($T_r = a_n^{gg}$) and that the tensile stiffness, J , of the geotextile is dependent on the normal stiffness of the contacts k_n^{gg} and the diameter of the particles d^g ($J = k_n^{gg} d^g$).

This membrane deformation under normal uniform pressure simulated with this method was compared with analytical solutions (Delmas 1979) and numerical solutions (Villard and Giraud 1998). The results obtained were approximately identical, thus validating the model chosen.

3.4 Determining the Parameters of the Soil-Geotextile Interface

The behavior of the interface between the soil and a geotextile is generally characterized, on the macroscopic level, by a friction law of the Mohr-Coulomb type. For problems involving large-scale plastic phenomena (large relative displacements of the zones in contact), the dominant parameter is the friction angle of the interface, δ , and its stiffness plays only a secondary role. There is no mathematical formula that can be used to establish the link between δ and the micro-mechanical models. The setting of the interface friction was thus carried out by simulating the pulling-out of a run-out anchor in which the direction of pulling was horizontal. Figure 11 presents the geometry of the model used for this type of calculation.

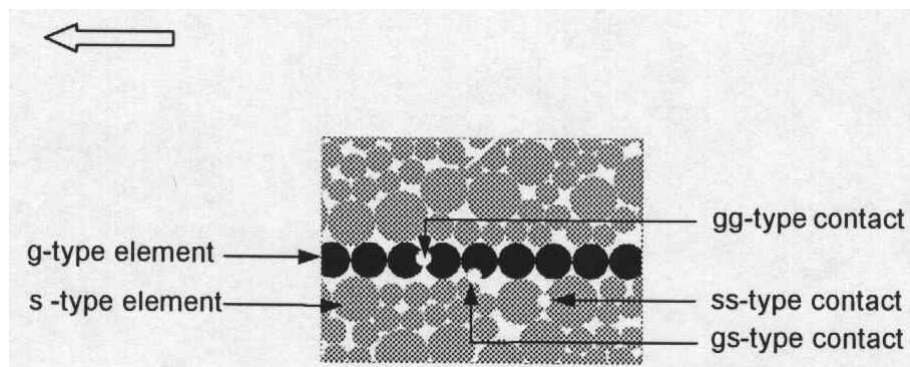


Figure 11. Modeling a run-out anchor.

The procedure for installing the particles for an anchorage test is similar to that presented for biaxial compression tests. The size of the soil particles was gradually increased, while the rigid walls (on the perimeter of the slope) and the particles of the geotextile were fixed. Porosity was modified by adjusting the inter-granular friction of the soil μ^{ss} . The size of the geotextile particles was such that its thickness remained small in relation to the dimensions of the model. Pull-out was simulated by imposing a displacement speed to the pull-out end. Comparative calculations showed that, for speeds of 2×10^{-3} to 2×10^{-4} m/s, the dynamic phenomena did not have a significant influence on the results of the calculation (quasi-static loading). All the results presented hereafter were obtained with a pull-out speed of 10^{-3} m/s.

Taken as a whole, the simulations performed show that friction, δ , depends mainly on the following: the local soil-geotextile friction, μ^{sg} ; the relative roughness, R , between the particles of the geotextile and those of the soil ($R = d^g / l_s$); and the local soil-soil friction, μ^{ss} (the shearing of the interface involves strains in the soil). As the parameters of the soil and the size of the particles had already been set at this stage, the only adjustable parameter was μ^{sg} .

The force-displacement curve obtained after adjusting μ^{sg} is compared in Figure 12, with the curve obtained in the experiment (W_Q is the weight of the soil covering the sheet). The modeling parameters selected for the soil, the geotextiles, and the soil-geotextile interface are given in Tables 4 and 5. By default, the parameters k_n^{sg} and k_s^{sg} (the normal and shear stiffness of the soil-geotextile contacts, respectively) were given the same values as those for the soil. The vectors of displacement of the particles between the initial and the final state are presented in Figure 13. One can observe that the modeled anchorage mechanism is similar to that observed experimentally, i.e., a combined displacement of the sheet and the soil cover. In these conditions, the interface located above the geotextile is subjected only to normal stress, while the lower interface is subjected to strong shear stress. A thin shear band forms under the sheet, dilates, and causes a slight vertical displacement of the soil cover.

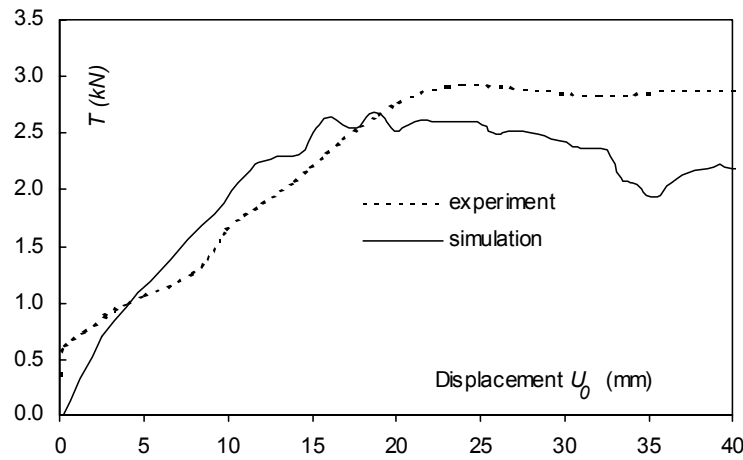


Figure 12. Experiment-modeling comparison for a run-out anchor.

Table 5. Parameters selected for modeling the geosynthetic and its interface.

Parameters selected for the geosynthetic	Value
Intrinsic characteristics of GTX ₁	
Tensile strength, a_n^{gs} (kN/m)	30
Shear strength, a_s^{gs} (kN/m)	30
Normal stiffness, k_n^{gs} (kN/m ²)	$80/d^g$
Shear stiffness, k_s^{gs} (kN/m ²)	0.5×10^5
Friction angle, μ^{gs}	0
Intrinsic characteristics of GTX ₂	
Tensile strength, a_n^{gs} (kN/m)	95
Shear strength, a_s^{gs} (kN/m)	95
Normal stiffness, k_n^{gs} (kN/m ²)	$624/d^g$
Shear stiffness, k_s^{gs} (kN/m ²)	0.5×10^5
Friction angle, μ^{gs}	0
Interface characteristics	
Relative roughness of interface, R	0.73
Tensile strength, a_n^{sg} (kN/m)	0
Shear strength, a_s^{sg} (kN/m)	0
Normal stiffness, k_n^{sg} (kN/m ²)	1×10^5
Shear stiffness, k_s^{sg} (kN/m ²)	0.5×10^5
Friction angle, μ^{sg} (°)	40.4

3.5 Influence of the Third Dimension

Generally, liners on slopes are longer than they are wide. This justifies the hypothesis of in-plane deformation and, thus, two-dimensional modeling of the problem. On the other hand, the experimental set-up presented did not maintain the two-dimensional aspect of the problem, as there could be friction between the sand and the side walls, even though the latter was covered with a smooth geomembrane. Although the ulti-

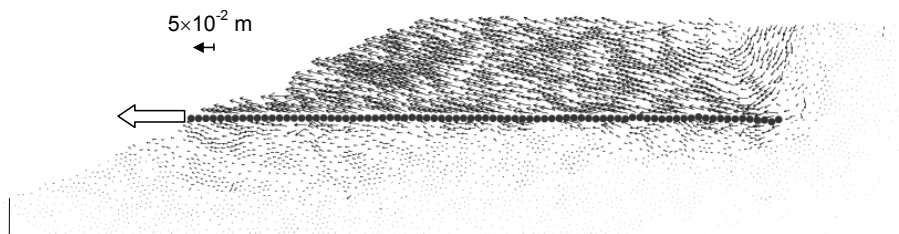


Figure 13. Particle displacement field for a run-out anchor ($U_0 = 0.04$ m).

mate objective of this work is to model actual structures, the comparison between the experiment and the simulation necessarily requires an assessment of the edge effects in the experiment; this is why the effect of lateral friction was included in the two-dimensional model even if there is no side wall effect in the actual cases. The reader is reminded that the soil cover (layer of soil of thickness H on top of the geotextile) was not subject to lateral friction since a space of 10 mm was left between this layer of soil and the side walls.

The model, initially based on the mechanics of continuous media, was adapted to discrete media using many hypotheses. Locally, it was assumed that the friction forces that could be mobilized between the sand and the side wall geomembrane obey Coulomb's Law (Equation 1), which is as follows:

$$\tau_{max} = \tan(\phi_{gmb/soil}) \sigma_n \quad (1)$$

where: τ_{max} = maximum shear stress; $\phi_{gmb/soil}$ = soil-geomembrane interface friction angle; and σ_n = applied normal stress.

The model proposed makes it possible for the friction at the interface to be gradually mobilized, due to Equation 2, which gives the increment in friction $d\tau$ in relation to the increment in displacement $d\vec{u}$. The stress vector of intensity is τ_{max} in the opposite direction to that of the displacement and u_{ref} is a variable (reference displacement) characterizing the flexibility of the interface. The displacement (and, consequently, friction) may change its direction, as well as its orientation, which is why the following relation is vectorial:

$$d\vec{\tau} = (\vec{\tau}_{max} - \vec{\tau}) \frac{\|d\vec{u}\|}{u_{ref}} \quad (2)$$

It should be noted that comparative calculations with u_{ref} varying between 10^{-2} and 10^{-3} m showed that the results were only very slightly sensitive to this parameter.

Figure 14 shows the changes in friction as given by Equation 2 for a rectilinear movement with a change in the direction of the displacement. In the case of a displacement in a constant direction, the convergence of τ toward τ_{max} is exponential. Due to its formulation, a change in the orientation of the displacement is not followed immediately by a change in the orientation of the stress, and τ gradually adapts to the displacement in the same way as the intensity. This gradual behavior is necessary if an

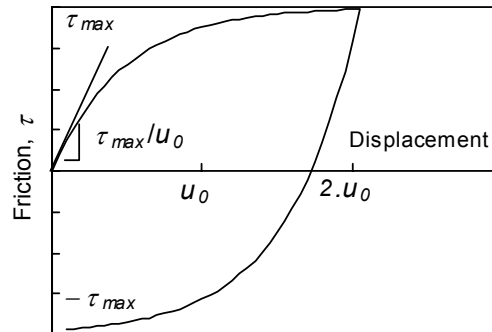


Figure 14. Modeling lateral friction (particular case of rectilinear movement).

accurate description is to be given of the lateral friction of the discrete model particles whose displacements are sometimes subject to rapid fluctuations in intensity and in direction.

The discrete model used was a two-dimensional problem with cylindrical particles. If the friction on the sides of the cylinders was to be taken into consideration, strong hypotheses needed to be formulated. As the discrete model does not allow the calculation of normal stress, σ_n , the normal stress was defined by analogy with a state of in-plane deformations by Equation 3:

$$\sigma_n = \nu(\sigma_1 + \sigma_2) \tag{3}$$

where: σ_1 and σ_2 = main stresses in the plane of reference; and ν = Poisson's ratio.

For each of the particles in the model, it was then possible, knowing the displacement \vec{u} and the stresses applied to it (average stresses obtained by an averaging procedure in the vicinity of the element), to calculate the stress τ_{max} and $d\tau$ using Equations 1 and 2. The friction on the element was simulated by applying a force \vec{F} equivalent to the sum of the lateral friction acting on these two ends. Equation 4 gives the increase $d\vec{F}$ in \vec{F} in relation to the increase in stress $d\tau$, where S is the surface area influenced by the particle, taking into account the average porosity, n , of the medium being studied ($S = s/(1 - n)$ with s being the lateral surface area of the particle:

$$d\vec{F} = 2S d\tau \tag{4}$$

The calculations corresponding to Equations 1 to 4 were performed for each element in the zone subject to edge effects. The total friction forces were updated in the course of the simulation using the following:

$$\vec{F}(t + dt) = \vec{F}(t) + d\vec{F}(t, dt) \tag{5}$$

where: t = time (of the simulation); and dt = a sufficiently small time step (the displacements of the particles during the interval dt must always to be less than $u_{ref}/10$).

4 COMPARISON OF THE NUMERICAL AND EXPERIMENTAL RESULTS

4.1 General

The numerical simulations were performed on models comprising approximately 8,000 particles. The model parameters used to reproduce the behavior of the materials in the experiment are given in Tables 4, 5, and 6. Tests with sandy silt were not simulated. Each of the results presented is the average result of four simulations (only the results of the particle displacement vectors come from calculations judged to be representative). The choice of the number of elements effects the particle size, but as long as the particle-size distribution (the ratio between the dimensions of the particles) remains unchanged, the size of the particles does not influence the calculations. In fact, it is easy to show, by a dimensional analysis, that subject to a homogenous stress conditions, the friction angle and the elastic properties obtained with DEM are independent of the element diameter. However, the size of the particles used must be sufficiently small in relation to the dimensions of the problem being studied. To provide a comparison, numerical simulations of the anchorage test were carried out with 4,000 and 8,000 particles. Similar behavior was observed in both cases (i.e., there was little change in the global kinetics and the average force-displacement curves) despite the fact that local differences, linked to the chosen discretization of the problem, were observed in the kinetics and in the force-displacement curves (which were more uneven).

4.2 Influence of β on Pull-Out Force

Numerical modeling was used to determine the influence of the slope angle β on the geotextile pull-out force. Several simulations were carried out for different values of β with the parameters relative to GTX₁. Figure 15 presents the particle displacement vectors (between the initial state and the final state) obtained in a representative simulation ($\beta = 28^\circ$). The $T_{max}(\beta) / T_{max}(\beta = 0)$ ratios in the numerical model are compared with those in the experiment in Figure 16, where $T_{max}(\beta)$ is the maximum tension (oriented in relation to the slope) required to pull out the sheet for a slope incline angle β . In Figure 16, there is a very close correlation between the experimental and modeling results.

Figure 16 also compares the experimental and modeling results with the analytical results obtained taking the angle effect into account (increase in anchorage capacity by the multiplicative factor $e^{\lambda \tan \delta}$). In this case, there are large differences between the results, especially for high β incline values because the analytical equation does not

Table 6. Parameters selected for modeling the side effects.

Side effect modeling parameter	Value
$\phi_{gmb-soil} (^\circ)$	20
$u_{ref} (m)$	2×10^{-3}
ν	0.3

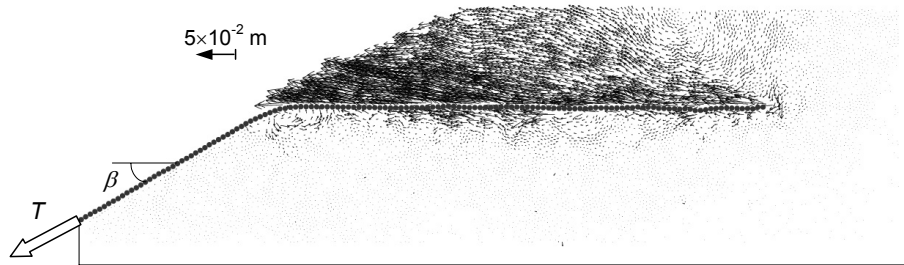


Figure 15. Particle displacement field for an anchor with tension applied along the slope ($\beta = 28^\circ$).

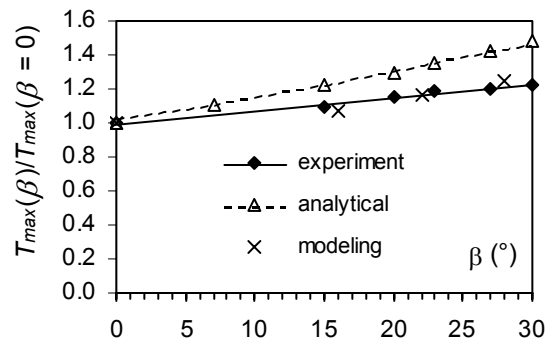


Figure 16. Influence of β on anchorage strength.

take into account compaction and/or failure of the soil on the corner.

4.3 Analysis of Anchor Trench Mechanisms

4.3.1 Introduction

The models proposed in this section refer to the S_2 (vertical embedding) and S_3 (L-shaped anchorage) tests carried out with the sand and GTX₂. For each case tested, two types of simulation were envisaged – one taking edge effects into consideration, the other not. Comparisons with the experimental results are made on the basis of the curves of the forces versus displacement at the pull-out end and of the deformation mechanisms.

4.3.2 Force-Displacement Curves

The experimental and theoretical curves of tension T at the pull-out end of the geotex-

tile in relation to the displacement of the end U_0 are compared for each of the modeled tests in Figures 17 and 18. At the beginning of each test, an acceptable correlation is observed between the model and the experiment. This phase of the test corresponds to the gradual tensioning of the horizontal section of the sheet. It was shown previously (the influence of angle β on the pull-out force) that the model can approximately reproduce the experimental results. The second part of the test corresponds to the tensioning of the end of the sheet (vertical section and/or horizontal section of the end of the sheet). In this case, it can be noted that the models underestimate the experimental anchorage capacity. The differences observed are a sign of the complexity of the mechanisms brought into play in this second stage of the test. The analysis of the anchorage mechanisms shows that the soil is strongly rounded out and sheared around the angles, thus indicating the important role played by the soil in global anchorage behavior.

Comparison of the experimental results with the existing design equations

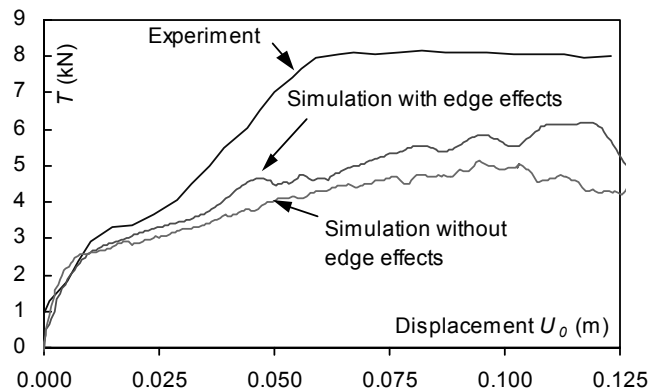


Figure 17. Results of the model of a vertical embedding anchor.

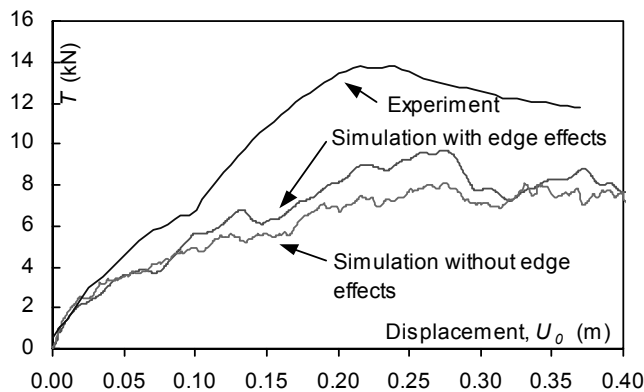


Figure 18. Results of the model of an L-shaped anchor.

(Briançon et al. 2000; Briançon 2001) shows that the latter generally overestimates anchorage capacities (even though the edge effects probably increase the strength measured in the experiments). The least well-suited analytical formulae are those that include the angle change formula that leads to an overestimation of the additional strength provided by the anchorage curvature. On the whole, the current analytical formulae do not take into consideration the soil characteristics and omit phenomena of rounding out, shear, and soil deformations that play a significant role in anchorage capacity.

4.3.3 Anchor Trench Deformation Mechanisms

The deformation mechanisms obtained on anchor trenches (vertical embedding and L-shaped anchors) are rather similar, taking into account the gradual tensioning of the sheet. Only the L-shaped anchor results will be analyzed in detail. Figure 19 shows the deformed geometry of the sheet for various stages of pull-out. Compared with the results of experimental test S₃, the movements of the sheet correspond well with the observed movements and are summarised as follows:

- $0 \text{ m} < U_0 < 0.04 \text{ m}$: the first horizontal segment is gradually begins to move. For $U_0 = 0.04 \text{ m}$, the upper section of the segment begins to move.
- $0.04 \text{ m} < U_0 < 0.12 \text{ m}$: the upper corner is progressively deformed and becomes more rounded, without significant movement of the rest of the sheet.
- $0.12 \text{ m} < U_0 < 0.24 \text{ m}$: gradual deformation of the second angle as it becomes more rounded and tensioning of the last segment of the sheet.
- $U_0 = 0.24 \text{ m}$: the end of the sheet begins to move.

Figure 20 shows the deformations of the soil mass at the end of the test ($U_0 = 0.24$

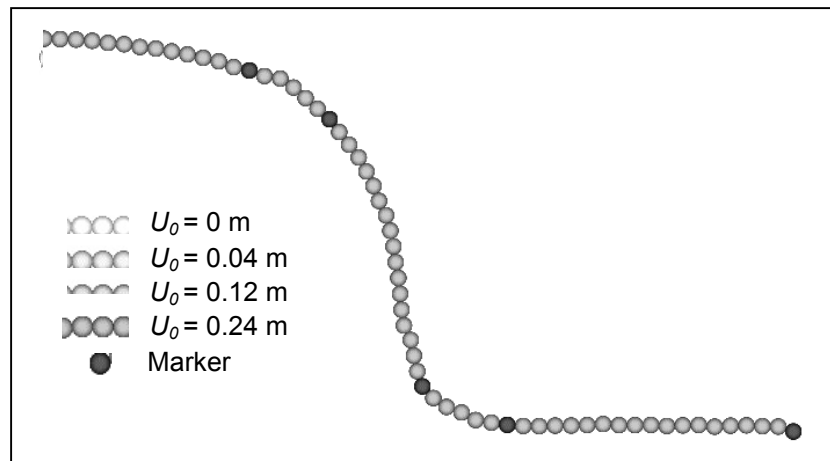


Figure 19. Deformed geometry of the sheet for different values of U_0 (true scale).

m). The soil columns, which were initially vertical, tilted during the test and highlight a shear zone in the soil (shaded zone). These results can be compared with the experimental results presented in Figure 7a, also showing shear zones in the soil. The location of the failure in the numerical model is more diffuse, for the thickness of the zone affected is closely linked to the dimensions of the modeled particles. However, at a qualitative level, the numerical model offers a good representation of the phenomena that are observed in the experiments.

4.4 Assessment of the Comparison Between the Models and Experiments

Comparisons between the experimental and theoretical results show that, in simple cases (run-out anchorage), the model and experimental results are approximately the same. In more complex cases (anchor trenches), certain disparities are observed, notably at the end of the tests when the mechanisms brought into play are complex.

Qualitatively, the mechanisms of anchorage behavior obtained by modeling are similar to those in the experiments (i.e., gradual tensioning of the sheet, rounding out of the soil at the corners, and lift and shear of certain parts of the soil mass).

Quantitatively, the models proposed (both with and without edge effects) systematically underestimate anchorage capacity. There may be several causes for the differences observed such as the following:

- Poor modeling of soil behavior, either in determining model parameters or in characterizing the soil (absence of cohesion).
- Poor characterization of the soil-geotextile interface behaviour. In particular, the calculations highlight a strain softening behavior of the interface, while the experimental behavior is similar to the perfectly plastic type. This strain softening behav-

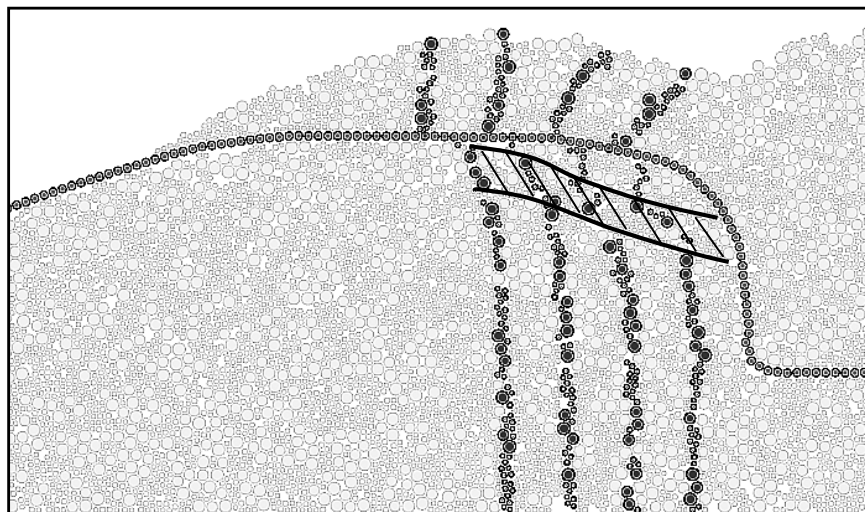


Figure 20. Soil deformation in an anchorage test ($U_0 = 0.24$ m)

ior is due to the fact that the failure is accompanied by a disconnection of the particles in the vicinity of the interface.

- Miscalculation of lateral friction. In fact, the model proposed for the edge effects was based on a large number of hypotheses and extrapolating two-dimensional results to a three-dimensional problem remains a delicate task. Complex mechanisms, such as the formation of arches between the two side walls were neglected. As a result, it is probable that edge effects were underestimated. However, these phenomena are only of secondary importance in that they are specific to the experiment and do not come into play in the behavior of the structures themselves.

5 CONCLUSIONS

The analysis of the experimental and theoretical results of the pull-out tests highlights certain essential aspects of the geotextile anchorage behaviour at the top of a slope. This analysis demonstrates, in particular, the following major roles of the soil in the failure mechanisms:

- failure of the soil mass along preferential slip lines (in the case of granular materials);
- rounding out of the soil at the points where there is a change in the angle of the geotextile; and
- large-scale deformation and displacement of certain sections of the soil mass.

When designing the anchorage, it is therefore not sufficient to merely take into consideration the geometry of the problem and the interface characteristics. It is essential to include soil failure mechanisms in the analytical formulae, which generally overestimate anchorage capacities, if the anchorage capacities are to be correctly assessed. Additional numerical and experimental studies must be carried out on this subject for different types of soils, other anchor shapes, and other geosynthetic products. However, it seems reasonable to consider that these conclusions could apply to geomembrane anchorages. Tensile force mobilization would require larger displacements, but pull-out strength, and failure mechanisms may be approximately the same supposing that the anchorage capacity does not exceed the tensile strength of the geomembrane.

The comparison experimental and modeling results show that the calculation method selected applies relatively well to modeling anchorage tests. Although the results are practically identical in simpler cases, some quantitative differences can be observed in more complex cases. In qualitative terms, however, the anchorage mechanisms are reproduced correctly by the Discrete Element Model, thus validating the choice of this model to estimate anchorage capacities. The main difficulty with this type of modeling resides in determining the parameters, a process that requires very precise adjustment and many calculations. Additional numerical studies must be performed if a better understanding of anchorage mechanisms are to be achieved, particularly for cohesive soils. Additional numerical studies should also enable improvement of the existing analytical formulae and more precise determination of anchorage capacities.

ACKNOWLEDGEMENTS

The authors thank C.E.T.M.E.F. for their participation and the producers (Bidim, O. Artières and Siplast, G. Potié, and A. Grisard), who provided geotextiles and geomembranes and contributed their own experience in the field of geosynthetic anchorage.

REFERENCES

- Briançon, L., 2001, “*Stabilité sur pentes des dispositifs géosynthétiques – Caractérisation du frottement aux interfaces et applications*”, Thèse de docteur ès Sciences, Université de Bordeaux I, Bordeaux, France, 200 p. (in French)
- Briançon, L., Girard, H., Poulain, D., and Mazeau, N., 2000, “Design of anchoring at the top of slopes for geomembrane lining systems”, *Second European Geosynthetics Conference*, Vol. 2, Bologna, Italy, October 2000, pp. 645-650.
- Cundall, P. and Strack, O.D.L., 1979, “A discrete numerical model for granular assemblies”, *Géotechnique*, Vol. 29, No. 1, pp. 47-65.
- Delmas, P., 1979, “*Sols renforcés par géosynthétiques – premières études*”, Thèse de l’université scientifique et médicale de Grenoble, Grenoble, France, 200 p. (in French)
- Guide technique, 2000, “*Étanchéité par géomembranes des ouvrages pour les eaux de ruissellement routier*”, co-édité par le SETRA et le LCPC, guide complémentaire, 71 p.
- Hryciw, R.D., 1990, “*Load Transfer Mechanisms in Anchored Geosynthetic Systems*”, *University of Michigan Research Report to the Air Force Office of Scientific Research*, Grant N° 88-0166, University of Michigan, Ann Arbor, Michigan, USA.
- Hulling, D.E. and Sansone, L.J., 1997, “Design concerns and performance of geomembrane anchor trenches”, *Geotextiles and Geomembranes*, Vol. 15, Nos. 4-6, pp. 403-417.
- Imaizumi, S., Tsuboi, M., Doi, Y., Shimizu, T., and Miyaji, H., 1997, “Anchorage ability of a geosynthetic liner buried in a trench filled with concrete”, *Proceedings of the Seventh International Waste Management and Landfill Symposium*, Sardinia 97, October 1999, S. Margherita di Pula, Cagliari, Sardinia, Italy, pp. 453-462.
- Koerner, R.M. and Wayne, M.H., 1991, “Mechanical and Hydraulic Testing of Geomembranes”, *Geomembrane Identification and Performance Testing*, RILEM Report 4, Rollin, A. and Rigo, J.M., Editors, Chapman and Hall, London, pp. 204-218.
- Koerner, R.M., 1998, “*Designing with Geosynthetics*”, Prentice Hall, Englewood Cliffs, New Jersey, USA, Fourth Edition, 761 p.
- NF P 84-522, 1994, “*Géomembrane – Mesure de l’angle de glissement des dispositifs d’étanchéité par géomembrane (DEG) à l’aide d’un plan incliné*”, French Standard, AFNOR, juin 1994, Paris, France. (in French)

- prEN ISO 12957-2, 2000, “*Geosynthetic – Determination of friction characteristics, Part 2: Inclined plane test*”, European Committee for standardisation (CEN), European Standard, September 2000, Brussels, Belgium.
- prEN ISO 12957-1, 2001-2002, “*Geotextile and geotextile-related products – Determination of friction characteristics, Part 1: Direct shear test*”, European Committee for standardisation (CEN), European Standard, Brussels, Belgium.
- Schneebeli, G., 1956, “Une analogie mécanique pour les terres sans cohésion”, *Comptes rendus de l’académie des sciences*, Vol. 243, No. 1, Archives de l’académie des sciences, Paris, pp. 125-126.
- Villard, P. and Giraud, H., 1998, “Three-dimensional modelling of the behaviour of geotextile sheets as membrane”, *Textile Research Journal*, Vol. 68, No. 11, pp. 797-806.

NOTATIONS

Basic SI units are given in parentheses.

a	= soil-geotextile adhesion (N/m ²)
a_n	= tensile strength of contacts (N/m)
a_n^{gg}	= tensile strength of contacts of geotextile (N/m)
a_n^{sg}	= tensile strength of contacts between soil and geotextile (N/m)
a_n^{ss}	= tensile strength of contacts in soil (N/m)
a_s	= shear strength of contacts (N/m)
a_s^{gg}	= shear strength of contacts of geotextile (N/m)
a_s^{sg}	= shear strength of contacts between soil and geotextile (N/m)
a_s^{ss}	= shear strength of contacts in soil (N/m)
B	= length of anchorage at bottom of trench (m)
c	= soil cohesion (N/m ²)
c'	= effective soil cohesion (N/m ²)
D	= length of vertical embedding (m)
d	= maximum diameter for a pair of particles (m)
d'	= minimum diameter for a pair of particles (m)
d^g	= diameter of particles used to model geotextile (m)
dt	= time step between each assessment of edge effects (s)
\vec{F}	= force resulting from friction on a particle (N)

H	=	thickness of soil cover above anchorage (m)
I_p	=	plasticity index (%)
J	=	tensile stiffness of geotextile (N/m)
K_0	=	coefficient of earth at rest (dimensionless)
k_n	=	tensile stiffness of contacts (N/m ²)
k_n^{gg}	=	tensile stiffness of contacts of geotextile (N/m ²)
k_n^{sg}	=	tensile stiffness of contacts between soil and geotextile (N/m ²)
k_n^{ss}	=	tensile stiffness of contacts in soil (N/m ²)
k_s	=	shear stiffness of contacts (N/m ²)
k_s^{gg}	=	shear stiffness of contacts of geotextile (N/m ²)
k_s^{sg}	=	shear stiffness of contacts between soil and geotextile (N/m ²)
k_s^{ss}	=	shear stiffness of contacts in soil (N/m ²)
L	=	upper horizontal segment of anchor (m)
l	=	length of an assembly (m)
l_1	=	length of small assemblies (m)
l_2	=	length of large assemblies (m)
n	=	porosity (dimensionless)
p	=	ratio of diameters of two particles in an assembly (dimensionless)
R	=	relative geotextile-soil roughness (dimensionless)
S	=	surface area influenced by particle (m ²)
s	=	surface area of side of cylindrical particle (m ²)
T	=	tensile force applied by traction cable (N)
T_h	=	horizontal component of T_{max} (N)
T_{max}	=	anchorage capacity (N)
T_r	=	tension at failure of geotextile (N/m)
\vec{u}	=	displacement of particle (m)
U_0	=	displacement of traction cable (m)
u_{ref}	=	reference displacement characteristic of interface flexibility (m)
V	=	compression speed in simulation of compression tests (m/s)
w	=	water content (%)

W_L	=	liquid limit (%)
W_P	=	plastic limit (%)
W_Q	=	weight of soil above geotextile sheet (N)
β	=	slope angle (°)
δ	=	soil-geotextile friction angle (°)
Δt	=	numerical resolution time step (s)
ϕ	=	internal friction angle of soil (°)
ϕ'	=	effective internal friction angle of soil (°)
$\phi_{gmb-soil}$	=	friction angle of soil on side walls (°)
γ	=	unit weight of soil (N/m ³)
γ_d	=	unit weight of dry sand (N/m ³)
λ	=	angle of change of direction of anchored geotextile (°)
μ	=	friction angle of contacts (°)
μ^{gg}	=	friction angle between two particles used to model geotextile (°)
μ^{ss}	=	friction angle of contacts in soil (°)
μ^{sg}	=	friction angle of contacts between soil and geotextile (°)
ν	=	Poisson's factor for soil (dimensionless)
σ_0	=	confinement stress when simulating biaxial compression (N/m ²)
σ_1	=	major principal stress (N/m ²)
σ_2	=	minor principal stress (N/m ²)
σ_h	=	horizontal stress on a vertical portion of geotextile sheet (N/m ²)
σ_n	=	normal stress (N/m ²)
σ_v	=	vertical stress on horizontal portion of geotextile sheet (N/m ²)
τ	=	magnitude of $\vec{\tau}$ (N/m ²)
$\vec{\tau}$	=	shear stress of the sand-geomembrane interface (N/m ²)
τ_{max}	=	magnitude of $\vec{\tau}_{max}$ (N/m ²)
$\vec{\tau}_{max}$	=	maximum shear stress of sand-geomembrane interface (N/m ²)